Underwater Acoustic Communication with an Orthogonal Signal Division Multiplexing Scheme in Doubly Spread Channels

Tadashi Ebihara, *Member, IEEE*, and Koichi Mizutani, *Non-member, IEEE*

***Abstract*— Underwater acoustic (UWA) communication is an ongoing challenge because of the heavy time spread by multipath and Doppler spreads. Here we propose a UWA communication system using orthogonal signal division multiplexing (OSDM), a scheme that measures the multipath profile without an adaptation or interpolation process, to achieve stable communication in doubly spread channels. We previously evaluated the performance of an OSDM scheme in a UWA communication system in both an experiment and simulations. In the present study, we experimentally compared the performance of OSDM and existing communication schemes — single-carrier with decision feedback equalizer (DFE) and orthogonal frequency division multiplexing (OFDM) — in a test tank with respect to communication quality, data rate, frame length, and calculation complexity. We found that OSDM with a multichannel receiver is attractive in terms of communication quality; it achieved a far better bit-error-rate (BER) performance compared to the other schemes in both static and dynamic channels with various input signal-to-noise ratios, although the complexity is less than that achieved with single-carrier DFE. Based on these findings, we suggest that OSDM can provide a highly reliable communication environment for UWA communication with multipath and Doppler spread, such as in shallow water.**

***Index Terms*—multipath, Doppler spread, underwater acoustic communication**

I. Introduction

UNDERWATER acoustic (UWA) communication is widely used in many applications and is a particularly critical technology for underwater exploration activities. Systems based on the phase-coherent modulation technique are intensively studied with the goal of increasing the bandwidth efficiency of UWA communication systems [1]. However, several problems present ongoing challenges for UWA communication. UWA channels, especially shallow-water ducts, are characterized by numerous encounters with both the sea surface and seafloor [2]. This multipath environment causes signal fading and intersymbol interference (ISI). The multipath-induced channel spread in time in a horizontal shallow-water duct can cause the ISI to extend to over a hundred symbols [3]. Moreover, the existence of the moving sea surface and the communication platform's movement cause a Doppler shift, and multiple Doppler-scaling paths and time variation of the UWA channel lead to Doppler spread. The ISI and Doppler spread can serve as a barrier to UWA communication, because the effect of ISI and Doppler spread can become several orders of magnitude greater than the one observed in a communication system using radio, considering the sound velocity underwater.

To achieve high-speed UWA communication in doubly spread (i.e., time-spread and Doppler-spread) channels, communication systems based on the phase-coherent modulation technique have been studied [4–26]. These systems employ equalization techniques, array processing, or a combination of these methods to overcome the ISI. For UWA communication systems, a single-carrier with an adaptive decision feedback equalizer (DFE) with a least mean squares (LMS) or recursive

Manuscript received January 14, 2011. This work was supported in part by the Japan Society for the Promotion of Science under Grant 24760672. T. Ebihara is a member of the Faculty of Engineering, Information and Systems, University of Tsukuba, Tsukuba, 305-8573 Japan (e-mail: ebihara@iit.tsukuba.ac.jp)

K. Mizutani is a member of the Faculty of Engineering, Information and Systems, University of Tsukuba, Tsukuba, 305-8573 Japan (e-mail: mizutani@iit.tsukuba.ac.jp)

least-squares (RLS) algorithm is usually employed to combat ISI [4–15]. A combination of DFE and array processing has also been found to achieve high-quality communication [7–13]. In terms of the Doppler effect, an interesting result has been reported; the communication performance is improved by increasing the transmission rate, which results in a more frequent observation of channels and reduction of the effect of Doppler spread [11]. For cases in which the Doppler spread becomes more severe, a receiver with a channel tracker that enables the tracking of Doppler spread has been proposed [14,15]. However, receiver complexity prevents a substantial improvement of the data rate. Existing equalizers require the following: a number of taps corresponding to the discretized baseband UWA channel taps, training periods to optimize the taps, and calculations for optimization. As the data rate increases, more taps are required. Although the LMS algorithm has an advantage in terms of calculation cost, it has a disadvantage with respect to convergence speed. That is, the training period lengthens and the effective data rate decreases. Conversely, RLS has an advantage in terms of convergence speed but a disadvantage with respect to calculation cost.

UWA communication using orthogonal frequency division multiplexing (OFDM) has attracted much attention and is considered a viable alternative due to the low complexity of the receiver [16–20]. Unlike DFE, which equalizes the received signal in a time domain, OFDM equalizes the received signal in a frequency domain, and only the complex multiplication for each subcarrier is required. A pilot signal, which is scattered in a time or frequency domain, is usually employed to obtain the channel information. However, interpolation is required to obtain the channel information. A densely arranged pilot signal improves the channel measurement accuracy; however, the effective data rate decreases. A sparsely arranged pilot signal improves the effective data rate, but the channel measurement error will be increased. In terms of the Doppler effect, inter-carrier interference occurs even in a small Doppler shift, and a receiver that deals with the Doppler effect has been considered [19,20].

We have focused on another scheme for UWA communication in shallow water: orthogonal signal division multiplexing (OSDM) [21–24]. OSDM has been proposed for mobile wireless communication to achieve reliable channel sensing. In terms of ISI, OSDM has an advantage compared to existing communication schemes: OSDM multiplexes several data vectors — a pilot signal as well as messages — into a single data stream, and it does not require any interpolation in the process of channel measurement. The equalization process is conducted frame-by-frame, and OSDM requires a matrix calculation which is expected to increase the calculation cost compared to OFDM, but its complexity is expected to be low compared to that of RLS-DFE, which requires iterative calculations in the process of channel estimation. We previously evaluated the performance of an OSDM scheme for ISI [25, 26], and we found that the OSDM achieves better communication quality than single-carrier LMS-DFE under the same data rate when the channel is static. In terms of Doppler effect, Doppler shift correction for OFDM [27], which exploits a guard interval, has been found to work well enough to enable reliable communication [28–30]. We performed the Doppler shift correction in a previous experiment and found that a smaller frame length is preferable because it enables the frequent measurement of the UWA channel and keeps up with channel changes [30]. However, a comparison of OSDM and existing communication schemes in doubly spread channels has not yet been reported, to our knowledge.

In the present study, to identify the characteristics of OSDM for UWA communication, we tested the OSDM scheme in a doubly spread channel by comparing its performance to that of existing schemes with single-carrier DFE and OFDM, in a test tank experiment with reverberation and surface waves and in simulation with reverberation and Doppler effects. We compare the performance of these schemes with respect to communication quality and calculation complexity, under the same data rate and the same signal bandwidth. The following Section II overviews the OSDM scheme. Section III compares the OSDM and existing schemes in simulation and experiment. Section IV presents our conclusions.

II. Orthogonal Signal Division Multiplexing

A. OSDM scheme in transmitter and receiver

Figure 1 shows block diagrams of OSDM in the transmitter and receiver in a baseband system. We consider N data vectors of length M, $\boldsymbol{x}_{tn}$ (n = 0, 1, …, N-1), as the transmission message. Each $\boldsymbol{x}_{tn}$ contains a different message whose elements are modulated symbols (e.g., QPSK) expressed as complex numbers. The N data vectors $\boldsymbol{x}_{tn}$ are multiplexed into a single data stream of length MN, $\boldsymbol{X}$, according to:

$$\boldsymbol{X} = \sum_{n=0}^{N-1} \boldsymbol{f}_{Nn} \otimes \boldsymbol{x}_{tn}\,, \tag{1}$$

where

$$F_N^{-1} \equiv \begin{pmatrix} \boldsymbol{f}_{N0} \\ \boldsymbol{f}_{N1} \\ \vdots \\ \boldsymbol{f}_{N(N-1)} \end{pmatrix} = \frac{1}{\sqrt{N}} \begin{pmatrix} W_N^0 & W_N^0 & \cdots & W_N^0 \\ W_N^0 & W_N^1 & \cdots & W_N^{N-1} \\ \vdots & \vdots & \ddots & \vdots \\ W_N^0 & W_N^{(N-1)} & \cdots & W_N^{(N-1)^2} \end{pmatrix}, \tag{2}$$

$$W_N^k = \exp\left(\frac{2\pi\sqrt{-1}k}{N}\right). \tag{3}$$

In Eq. (1), "$\otimes$" denotes the Kronecker product, and each $\boldsymbol{f}_{Nn}$ corresponds to a row of the inverse discrete Fourier transform matrix, F_N^{-1}. Note that $\boldsymbol{X}$ corresponds to an interleaved signal in direct-sequence code-division multiple-access (DS-CDMA) [31], as well as a signal in OFDM if M equals 1. If the maximum channel delay is L symbols, the transmission data stream, namely frame, $\tilde{\boldsymbol{X}}$, is obtained by prepending a cyclic prefix in which the last part of $\boldsymbol{X}$ with a length of L is placed at the beginning of $\boldsymbol{X}$, as follows:

$$\tilde{\boldsymbol{X}} = \begin{pmatrix} X[MN-L] & X[MN-L+1] & \cdots & X[MN-1] & \boldsymbol{X} \end{pmatrix}. \tag{4}$$

Note that L corresponds to a correctable channel reverberation time in a discrete model, and $L \le M$. The transmission data stream, $\tilde{\boldsymbol{X}}$, is transmitted through the channel. In the receiver, we consider that the receiver employs a single transducer (single-channel) for simplicity; K = 1 in Figure 1b where K is the number of array elements in the receiver. The received data stream from the channel, $\tilde{\boldsymbol{Y}}^0$, can be expressed using $\tilde{\boldsymbol{X}}$ and a channel response of length L, $\boldsymbol{h}^0$, as:

$$\tilde{\boldsymbol{Y}}^0 = \boldsymbol{h}^0 * \tilde{\boldsymbol{X}}\,, \tag{5}$$

where "$*$" denotes a convolution. There is a relationship between the cyclic-prefix-removed sequence, $\boldsymbol{Y}^0$, the channel response $\boldsymbol{h}^0$, and multiplexed data stream, $\boldsymbol{X}$, as:

$$\boldsymbol{Y}^0 = \boldsymbol{X}\begin{pmatrix} h^0[0] & h^0[1] & \cdots & h^0[MN-1] \\ h^0[MN-1] & h^0[0] & \cdots & h^0[MN-2] \\ \vdots & \vdots & \ddots & \vdots \\ h^0[1] & h^0[2] & \cdots & h^0[0] \end{pmatrix}, \tag{6}$$

where

$$\boldsymbol{Y}^0 = \begin{pmatrix} \tilde{Y}^0[L] & \tilde{Y}^0[L+1] & \cdots & \tilde{Y}^0[L+MN-1] \end{pmatrix}. \tag{7}$$

The relationship between $\boldsymbol{Y}^0$ and $\boldsymbol{x}_{tn}$ is expressed by the following equation:

$$\boldsymbol{Y}^0 D_n = \boldsymbol{x}_{tn} C_n^0, \tag{8}$$

where

$$D_n = \boldsymbol{f}_{Nn}^* \otimes I_M, \tag{9}$$

$$C_n^0 = \begin{pmatrix} h^0[0] & h^0[1] & \cdots & h^0[M-1] \\ \overline{W_N^n} h^0[M-1] & h^0[0] & \cdots & h^0[M-2] \\ \vdots & \vdots & \ddots & \vdots \\ \overline{W_N^n} h^0[1] & \overline{W_N^n} h^0[2] & \cdots & h^0[0] \end{pmatrix}, \tag{10}$$

and I_M is an M-by-M identity matrix, $\boldsymbol{f}_{Nn}^*$ is a complex conjugate of the transposition of $\boldsymbol{f}_{Nn}$, $\overline{W_N^n}$ is a complex conjugate of W_N^n, and $h[l]$ ($l = L, L+1, \ldots, M-1$) is zero. The Kronecker product, D_n, is prepared in the receiver before communication, and is called the matched filter. We define the matched-filter-operated sequences as $\boldsymbol{y}_n^0$. If $n = 0$, the relationship between $\boldsymbol{Y}^0 D_n$ and $\boldsymbol{x}_{t0}$ becomes:

$$\boldsymbol{Y}^0 D_0 = \boldsymbol{x}_{t0}\begin{pmatrix} h^0[0] & h^0[1] & \cdots & h^0[M-1] \\ h^0[M-1] & h^0[0] & \cdots & h^0[M-2] \\ \vdots & \vdots & \ddots & \vdots \\ h^0[1] & h^0[2] & \cdots & h^0[0] \end{pmatrix}. \tag{11}$$

If $\boldsymbol{x}_{t0}$ is shared by the transmitter and receiver, and its periodic autocorrelation function becomes an impulse according to:

$$\frac{1}{M}\boldsymbol{x}_{t0}\begin{pmatrix} \overline{x_{t0}}[0] & \overline{x_{t0}}[M-1] & \cdots & \overline{x_{t0}}[1] \\ \overline{x_{t0}}[1] & \overline{x_{t0}}[0] & \cdots & \overline{x_{t0}}[2] \\ \vdots & \vdots & \ddots & \vdots \\ \overline{x_{t0}}[M-1] & \overline{x_{t0}}[M-2] & \cdots & \overline{x_{t0}}[0] \end{pmatrix} = \begin{pmatrix} 1 \\ 0 \\ \vdots \\ 0 \end{pmatrix}, \tag{12}$$

the receiver can then obtain the channel response by calculating the periodic cross-correlation function between $\boldsymbol{y}_0^0$ and $\boldsymbol{x}_{t0}$ as:

$$\frac{1}{M}\boldsymbol{Y}^0 D_0 \begin{pmatrix} \overline{x_{t0}[0]} & \overline{x_{t0}[M-1]} & \cdots & \overline{x_{t0}[1]} \\ \overline{x_{t0}[1]} & \overline{x_{t0}[0]} & \cdots & \overline{x_{t0}[2]} \\ \vdots & \vdots & \ddots & \vdots \\ \overline{x_{t0}[M-1]} & \overline{x_{t0}[M-2]} & \cdots & \overline{x_{t0}[0]} \end{pmatrix} = \begin{pmatrix} h^0[0] & h^0[1] & \cdots & h^0[M-1] \end{pmatrix}. \tag{13}$$

Using the channel response obtained from the pilot signal, $\boldsymbol{x}_{t0}$, the receiver can calculate the matrix, C_n^0. We can then obtain the received message, $\boldsymbol{x}_{rn}$, by solving:

$$\boldsymbol{x}_{rn} = \boldsymbol{Y}^0 D_n \left(C_n^0\right)^{-1}. \tag{14}$$

In the following, we use:

$$x_{t0}[m] = \exp\left(\frac{2\pi\sqrt{-1}m^2}{M}\right), \ (m = 0, 1, \ldots, M\text{-}1), \tag{15}$$

whose periodic cross-correlation function becomes an impulse, as $\boldsymbol{x}_{t0}$.

From Eqs. (8) and (14), the accuracy of the received message, $\boldsymbol{x}_{rn}$, depends on the condition number of C_n^0. Figure 2 shows the histogram of the condition number — the ratio of the largest singular value of C_n^0 to the smallest one — assuming that the channel, $\boldsymbol{h}^0$, is the Rayleigh fading channel of $L = 60$ with an exponentially decaying (0.33 dB per tap) power profile when $M = 63$ and $N = 2$. In case of the single channel ($K = 1$), as shown in Figure 2, the expected value and the variance of the condition number of C_n^0 is large and the noise enhancement due to the ill-condition of C_n^0 is expected. Although this ill-condition problem results in communication quality deterioration, the problem has remained unsolved. It occurs not only underwater but also in radio communication, but is more severe underwater than in radio communication due to a large L from the long reverberation time of the UWA channel. To cope with this problem, we propose the use of a multichannel receiver [29]. When the receiver employs K array elements, cyclic-prefix-removed sequences, $\boldsymbol{Y}^0$, $\boldsymbol{Y}^1$, …, $\boldsymbol{Y}^{K\text{-}1}$, are obtained. Assuming that the channel profile between the transmitter and the array element #k ($k = 0, 1, \ldots, K\text{-}1$) as $\boldsymbol{h}^k$, the relationships between $\boldsymbol{Y}^0$, $\boldsymbol{Y}^1$, …, $\boldsymbol{Y}^{K\text{-}1}$ and $\boldsymbol{x}_{tn}$ are expressed by the following equation:

$$\begin{pmatrix} \boldsymbol{Y}^0 D_n & \boldsymbol{Y}^1 D_n & \cdots & \boldsymbol{Y}^{K-1} D_n \end{pmatrix} = \boldsymbol{x}_{tn} C_n^{\mathrm{c}}, \tag{16}$$

where

$$C_n^{\mathrm{c}} = \begin{pmatrix} C_n^0 & C_n^1 & \cdots & C_n^{K-1} \end{pmatrix}. \tag{17}$$

By multiplying the pseudo-inverse matrix, $C_n^{c*}\left(C_n^{c}C_n^{c*}\right)^{-1}$, to Eq. (16) from the right side, the received message, $\boldsymbol{x}_{rn}$, can be obtained.

$$\left(\boldsymbol{Y}^{0}D_n \quad \boldsymbol{Y}^{1}D_n \quad \cdots \quad \boldsymbol{Y}^{K-1}D_n\right)C_n^{c*}\left(C_n^{c}C_n^{c*}\right)^{-1} = \boldsymbol{x}_{rn} \tag{18}$$

In Figure 2, we also show the histogram of the condition number of C_n^{c} when K = 2, 3, and 4, assuming that $\boldsymbol{h}^0$, $\boldsymbol{h}^1$, …, $\boldsymbol{h}^{K-1}$ are independent of each other. It seems that the condition number becomes small as K increases. With this finding, the use of a multichannel receiver for OSDM communication seems to be effective to cope with the ill-condition problem, in exchange for receiver complexity.

B. Characteristics, data rate, channel coherence time, and complexity of OSDM

We first focus on the characteristics of OSDM before considering the data rate, the required channel coherence time, and its complexity. The spectrum of OSDM signal can be obtained by computing the Fourier transform of $\boldsymbol{X}$ [32]. By assuming that the discrete Fourier transform matrix of $MN \times MN$ is:

$$F_{MN} \equiv \left(\boldsymbol{f}_{MN\,0}^{*} \quad \boldsymbol{f}_{MN\,1}^{*} \quad \cdots \quad \boldsymbol{f}_{MN\,(MN-1)}^{*}\right) = \frac{1}{\sqrt{MN}}\begin{pmatrix} W_{MN}^{0} & W_{MN}^{0} & \cdots & W_{MN}^{0} \\ W_{MN}^{0} & W_{MN}^{MN-1} & \cdots & W_{MN}^{1} \\ \vdots & \vdots & \ddots & \vdots \\ W_{MN}^{0} & W_{MN}^{(MN-1)^2} & \cdots & W_{N}^{MN-1} \end{pmatrix}, \tag{19}$$

the Fourier transform of $\boldsymbol{X}$ become $\left(Z_0 \quad Z_1 \quad \cdots \quad Z_{MN-1}\right)$, where

$$Z_q = \frac{1}{\sqrt{M}}\left(\boldsymbol{x}_{\mathrm{tr}} \quad 0 \quad 0 \quad \cdots \quad 0\right)\boldsymbol{f}_{MN\,q}^{*}, \ (q = 0, 1, \ldots, MN\text{-}1.\ r = \mathrm{mod}(q, N)). \tag{20}$$

From Eq. (20), it is clear that the spectrum of $\boldsymbol{x}_{tn}$ periodically appears for M times in the spectrum of $\boldsymbol{X}$. Unlike OFDM, in which the spectrum of $\boldsymbol{x}_{\mathrm{t}n}$ (M = 1) appears on a unique subcarrier, OSDM is expected to be robust against the deep-fading of the channel response in the frequency domain, considering that the OSDM combines M-subcarriers information for equalization.

In OSDM, the parameters L, M, and N are determined as follows. First, the duration time of elements of $\tilde{\boldsymbol{X}}$ (symbol time), T, is determined. By considering the channel reverberation time and T, L is calculated by discretizing the channel reverberation time. M and N are determined by considering the data rate, frame length, and complexity. The efficient data rate becomes $\frac{b \cdot M(N-1)}{(MN+L)T}$, where b is the number of bits in one symbol (e.g., b = 2 in QPSK), because $\boldsymbol{x}_{\mathrm{t}0}$ is devoted to the pilot and the cyclic prefix of length L does not contain original information. The frame length, which indicates the length of the transmitting data stream in time, becomes $(MN+L)T$. This frame length corresponds to the required channel coherence time because OSDM assumes that the channel is coherent during the transmission of $\tilde{\boldsymbol{X}}$, as indicated in Eqs. (5) and (6).

Next, we focus on the calculation complexity of OSDM. As shown above in Section II.A, OSDM requires signal processing in both the transmitter and receiver. We calculated the required complex multiplications and complex additions in both the

transmitter and receiver. As a result, the required number of complex multiplications for the OSDM receiver is about $KN\left(M^3+M^2\right)$. More specifically, OSDM requires MN complex multiplications and $MN(N-1)$ complex additions in the transmitter, and $\left(K+\frac{5}{6}\right)(N-1)M^3+\left[\left(\frac{3}{2}K+2\right)(N-1)+K\right]M^2+\left[K-\left(\frac{1}{2}k+\frac{5}{6}\right)(N-1)+KN^2\right]M$ complex multiplications and $\left(K+\frac{4}{3}\right)(N-1)M^3+\left[\left(K-\frac{3}{2}\right)(N-1)+K\right]M^2+\left[\left(KN-\frac{11}{6}\right)(N-1)-K\right]M$ complex additions in the receiver. The signal calculation in the transmitter is indicated in Eq. (1), which requires *MN* multiplications and *MN*(*N*-1) additions to calculate the Kronecker product from $\boldsymbol{f}_n$ and $\boldsymbol{x}_n$ and to calculate the sum of *N* Kronecker products, respectively. The receiver calculates the left side of Eq. (16), $\boldsymbol{Y}^k D_n$; $KN\cdot MN$ multiplications and $KN\cdot M(N-1)$ additions are required to calculate $\boldsymbol{Y}^k D_n$ for all *k* and *n*. By using the $\boldsymbol{Y}^k D_0$, channel responses, $\boldsymbol{h}^k$, are obtained in Eq. (13); $K\cdot M(M+1)$ multiplications and $K\cdot M(M-1)$ additions are required to calculate the right-hand side to obtain $\boldsymbol{h}^k$, for all *k*. The channel matrix in Eq. (17) is then calculated with the obtained channel responses; $K(N-1)\cdot\frac{M(M-1)}{2}$ multiplications are required to calculate C_n^k for all *k* and *n* = 1, 2, …, *N*-1. The receiver finally obtains the received message by calculating Eq. (18); $(N-1)\cdot KM^3$ multiplications and $(N-1)\cdot M^2(KM-1)$ additions are required to calculate $C_n^{\mathrm{c}}C_n^{\mathrm{c}*}$ for *n* = 1, 2, …, *N*-1; $(N-1)\cdot\left(\frac{5}{6}M^3+M^2-\frac{5}{6}M\right)$ multiplications and $(N-1)\cdot\left(\frac{4}{3}M^3-\frac{3}{2}M^2+\frac{1}{6}M\right)$ additions are required to calculate the inverse of $\left(C_n^{\mathrm{c}}C_n^{\mathrm{c}*}\right)^{-1}$ by Gaussian elimination for *n* = 1, 2, …, *N*-1; and $(N-1)\cdot\left(KM^2+M^2\right)$ multiplications and $(N-1)\cdot\left[M(KM-1)+M(M-1)\right]$ additions are required to calculate the left side for *n* = 1, 2, …, *N*-1.

The relationships among the data rate, frame length, and complexity of OSDM can be inferred from their respective equations shown in Table I. We can increase the data rate by increasing *M* and *N*, at the expense of increasing the frame length and complexity. Considering that the frame length increases linearly with *M* and *N*, and that the complexity increases with M^3 and *N*, increasing *N* effectively increases the data rate. Although using a multichannel receiver for OSDM is effective to cope with the ill-condition problem, the receiver complexity increases in proportion to *K*.

C. Existing UWA communication schemes

To identify the characteristics of OSDM for UWA communication, we selected existing schemes, i.e., single-carrier DFE and OFDM, for a performance comparison. To make a fair comparison of these schemes with respect to communication quality and calculation complexity, we equalized the data rate, the frame length, and the signal bandwidth of the schemes as described below. First, the signaling structure for OSDM, single-carrier DFE, and OFDM were defined as shown in Figure 3. Note that there is an assumption that the symbol time, *T*, for OSDM and for single-carrier DFE and the sample (sub-symbol) time, T_s, for OFDM are equal. Citing Figure 3, we provide an overview of the existing schemes in the following paragraphs.

1) Single-carrier DFE

Here we focus on a single carrier that uses RLS-DFE, because LMS-DFE has been found to require on the order of a thousand symbols to converge, in both experiments and simulation. In UWA communication with single-carrier DFE, the signal mainly consists of three parts: the training sequence, the message, and the un-signalized interval, and we call the combination of the three parts the "frame." We show the equations for the data rate, frame length, and complexity of RLS-DFE in Table I. In UWA communication with RLS-DFE, a message of length *B* is transmitted following a training sequence of length *A*. An un-signalized interval of length *C* is adopted to avoid the interference between frames. The receiver obtains the message with aid of DFE. Here we examined multichannel RLS-DFE, as shown in Figure 4. RLS-DFE requires a number of

calculations on the order of $\frac{5}{2}R^2+\frac{9}{2}R$ per single iteration, where R is the number of the DFE taps [33]. The DFE consists of a feedforward (FF) filter, a decision device, and a feedback (FB) filter (Fig. 4). When the maximum channel delay is L symbols in length and the receiver employs K array elements, the required taps for FF and FB filters become $K(L+1)$ and L, respectively, which means that R equals $K(L+1)+L$ [34]. Note that the convergence speed of RLS is sensitive to its forgetting factor. Assuming that RLS-DFE updates its tap value of FF and FB even in the message section of the frame using a decision-direct mode, we show the calculation cost of RLS-DFE per frame in Table I, in which $(A+B)$ iterations are performed to optimize RLS-DFE. Later, we compare the overall cost of OSDM and single-carrier DFE based on our experimental results.

2) OFDM

In UWA communication with OFDM, the signal consists mainly of two parts: the OFDM symbol and the guard interval, and we call the combination of these two parts the frame. Here, the guard interval is considered the cyclic prefix, as it is in OSDM. We show the equations for the data rate, frame length, and complexity of OFDM in Table I. The OFDM symbol, which employs PQ subcarriers, is transmitted following a cyclic prefix of length L samples. The subcarrier spacing, Δf, is defined as $1/(PQT_s)$. We consider two types of pilot allocation: block-type and comb-type, as shown in Figure 5. For block-type pilot allocation, the OFDM symbol for channel estimation, in which all subcarriers are used as pilots, is transmitted every Q symbols. For comb-type pilot allocation, P subcarriers are uniformly inserted into the OFDM symbol as pilot with Q subcarriers apart from each other. We examined an OFDM receiver with maximal ratio combining (MRC), as shown in Figure 6. The receiver removes the cyclic prefix, converts the PQ samples from serial to parallel (S-P), and performs FFT for each branch. For the block-type, the obtained channel response in the frequency domain is used in the following Q-1 symbols. For the comb-type, the receiver estimates the channel response at data subcarriers from P pilots with low-pass interpolation, in which the mean-square error between the interpolated points and their ideal values are minimized. When the receiver employs K array elements, the decision variable at the output of the MRC becomes:

$$X_{OFDM\_R}[p]=\frac{\sum_{k=0}^{K-1}Y_{OFDM}^{k}[p]\overline{H}^{k}[p]}{\sum_{k=0}^{K-1}\left|H^{k}[p]\right|^{2}},\quad (p=0,1,\ldots,PQ\text{-}1), \tag{21}$$

where Y_{OFDM}^{k} and $H^{k}[p]$ are the demodulated OFDM symbol and channel response in the frequency domain, on the array element #k at p-th subcarrier, respectively. Converting the decision variable sequence from parallel to serial (P-S), the receiver obtains the message. Considering that the Cooley-Tukey FFT with block-length of PQ requires $\frac{1}{2}PQ\log_2 PQ$ complex multiplications and $PQ\log_2 PQ$ complex additions, the required number of complex multiplications for the OFDM receiver is about $\frac{1}{2}KPQ\log_2 PQ$. Note that the calculation cost for channel interpolation is not considered. Later, we compare the overall costs of OSDM and OFDM based on our experimental results.

III. Performance Comparison of OSDM, Single-carrier DFE, and OFDM

A. Overview of the experiment and simulation

In this section, we evaluate the performance of OSDM, single-carrier DFE, and OFDM in an experiment and a simulation. For the experiment, we used a test tank with a wave generator. For the simulation, we used an equivalent baseband model whose channel properties were as close as possible to the channel properties in the experiment, so that we could confirm the experimental results. The testing environment is expressed in Section III.B below. We evaluated the performance of the three communication schemes in a static channel, in which the effect of noise and multipath are considered. In Section III.C, the performance of the communication schemes in various input signal-to-noise ratios (ISNRs) in a static channel is evaluated. Then, we evaluated the performance of the communication schemes in a dynamic channel, in which the effect of a moving surface (wave) by the wave generator is considered in addition to noise and multipath (Section III.D), and the performance of communication schemes in various ISNR and Doppler spread conditions is evaluated.

In this paper, ISNR and Doppler spread width, f_d, are employed to express the channel parameter, and output signal-to-noise ratio (OSNR) [7] and bit-error-rate (BER) are employed to express the performance of the communication schemes. In our experiment, the ISNR was defined as $(\sigma_s^2 - \sigma_n^2) / \sigma_n^2$, where σ_s^2 and σ_n^2 are the power of the received sequence (e.g., $\boldsymbol{Y}^0$) and the power of the received sequence when there are no signals, assuming that the signal and the noise are independent. In the simulation, ISNR was defined as the ratio between the power of the received sequence (the effects of multipath and Doppler spread are considered) and the additive noise. Because the amplitude of the output signal from the transmitter is normalized to avoid the saturation of the amplifier, the ISNR of OSDM is used to express the ISNR, although the ISNRs in OSDM, single-carrier DFE, and OFDM are different (see Section III.B).

B. Testing environment

The testing environment for the experiment is shown in Figure 7a. To conduct UWA communication, one transducer, Tx, (H1a, Aquarian Audio Products, Anacortes, WA, USA) and four transducers, Rx #1 to #4, (H2a, Aquarian Audio Products) were placed in the tank. Tx was connected to the transmitter and acted as the radiator. The other transducers were connected to the receiver and acted as the hydrophone. Before conducting UWA communication, we measured the channel responses by transmitting chirp signals of 1-s duration whose frequency was swept from 5 to 35 kHz, and by calculating the cross-correlation functions between the transmitted and received signals. Figure 7b and c show the measured channel response in the time domain and in the frequency domain, respectively. As indicated in Figure 7b, the obtained channel responses appear to be on the scale of 10 ms, requiring about 12 ms to decay the signal amplitude 20 dB from its peak. This convergence time is used to determine L. In the following experiment, we set T and T_s as 0.2 ms, which results in $L = 60$. From Figure 7c, the effect of the multipath can be confirmed as frequency-selective fading with deep fades. To test the experimental results, we conducted a simulation with an equivalent baseband model. In this simulation, the channel is expressed in as time-discrete, symbol-spaced (OSDM and single-carrier) or sample-spaced (OFDM). The channel is assumed to have be Rayleigh-distributed with and exponentially decaying (0.33 dB per tap), considering the channel decay observed in the experiment.

In the experiment, the transmission data stream (e.g., $\tilde{\boldsymbol{X}}$) was calculated. These complex symbols were divided into a real part and an imaginary part. For OSDM and single-carrier DFE, a raised cosine roll-off filter, whose roll-off rate is 0.5, was used for pulse-shaping. The symbol time T was determined as 0.2 ms, which is the same as the sample time T_s for OFDM. These output signals (the real and imaginary parts) are combined by modulation by two orthogonal carrier wave signals of the same frequency (20 kHz). The receiving signal was band-pass filtered, down-converted by orthogonal demodulation, and sampled at the timing of T or T_s. The sampled complex data stream (e.g., $\tilde{\boldsymbol{Y}}^0$) was then processed to obtain the message.

Figure 8 shows the spectra of the received signals of OSDM, single-carrier, and OFDM; the background noise level was set as 0 dB. In light of these results, the spectrum of OFDM with its rectangular shape is preferable in terms of spectral utilization. The spectra of OSDM and single-carrier DFE have a roll-off shape.

As shown in Table II, two trials (Cases #1 and #2) were performed. The message was defined as a QPSK-modulated sequence. The frame length, efficient data rate, and signal bandwidth in OSDM, single-carrier DFE, and OFDM were the same in each case. Note that the parameter C of single-carrier DFE (un-signalized interval between frames) in Case #1 is zero. C is preferable to the same value of L to avoid the interference between frames; this is to ensure enough training time for RLS-DFE without changing the data rate and frame length. Figure 9 shows the performance of RLS-DFE, whose forgetting factor is 0.98, obtained in the simulation and the experiment. The figure shows that RLS-DFE required a training sequence of a length of more than 120 symbols to converge a sufficient OSNR. As a result, in Case #1, the length of C is devoted to training and the tap value of the DFE is not reset and held in subsequent frames (re-training is performed in each frame). In Case #2, the tap value of the DFE is reset and re-training is performed in each frame.

We considered the number of array elements for the receiver, K, in the simulation and the experiment. Figure 10 shows the relationship between K and OSNR; Figure 10a and b provides the experimental and simulation results in Case #1 when the ISNR of OSDM was 30.3 dB. Figure 10c and d are the results in Case #2 when the ISNR of OSDM was 28.0 dB. With the relevant data from the experiment, we found that the OSNR becomes saturated as the K increases, and the simulation results support the experimental results. We therefore focused on $K = 1$ and $K = 3$ for single-channel and multichannel cases, respectively, considering the communication quality and receiver complexity, which increases with K. When $K = 1$, Rx #1 was used and when $K = 3$, Rx #1, #2, and #4 were used, because the ISNR of these are almost the same.

We also analyzed the peak-to-average power ratio (PAPR) of OSDM and OFDM, because the amplitude of the output signal from the transmitter was normalized (in the following subsections). Figure 11 shows the histograms of PAPR of OSDM and OFDM obtained in the simulation. Because the OSDM sequence is the sum of N sequences, which consists of QPSK symbols with phase-rotation by $\boldsymbol{f}_{Nn}$ as shown in Eq. (1), the maximum PAPR become N. As shown in Figure 11a, we found that the PAPR of OSDM became almost N because the number of N was small ($N = 2$ or 4) in this simulation. In OFDM, which employs PQ subcarriers, the maximum PAPR is known to become PQ. However, it is also known that the PAPR distributes when the number of PQ is large, as shown in Figure 11b.

Because the amplitudes of OSDM, single-carrier DFE and OFDM were normalized, the ISNRs of these schemes became different, as shown in Table III. In the simulation, the ISNR of OSDM was larger than that of OFDM and lower than that of single-carrier DFE, and the difference reflects the existence of the PAPR. However, the ISNR difference that we obtained in the experiment is different from the simulation results. This is due to the effect of the raised cosine roll-off filter. As mentioned in Section III.B, a raised roll-off cosine filter was used to shape the signal in the transmitter for OSDM and single-carrier DFE. Figure 12 shows the output of the transmitter when OSDM and single-carrier DFE sequences were input. Although the amplitudes of the input sequence of OSDM and single-carrier DFE were normalized, the amplitude of the output signal of single-carrier DFE jumps to about $\sqrt{2}$. This means that the single-carrier also has a PAPR in terms of passband-signal, and this results in the difference between the simulation and experimental results. In the following subsections, the wording "the ISNR" indicates the ISNR of OSDM, for convenience; however, note that the actual ISNRs for single-carrier DFE and OFDM are different owing to amplitude normalization.

C. Performance comparison in a static channel with various ISNRs

We evaluated the performance of OSDM, single-carrier DFE, and OFDM in a static channel, in which the effects of multipath and noise become problematic. The communication was performed in a test tank (Fig. 7a) by varying the amplitude of the signal, which resulted in different ISNRs. In the experiment, the signal frame which contains random information was

transmitted continuously for 100 and 32 frames for Cases #1 and #2, respectively. The communication was performed five times for each ISNR.

Figures 13 and 14 show the experimental and simulation results in Cases #1 and #2, respectively. First, we focused on the effect of a multichannel receiver for OSDM. By comparing the single-channel (Figs. 13a, 14a) and multichannel case (Figs. 13c, 14c), we saw that the performance of multichannel OSDM was greatly improved compared to that of the single-channel, and the use of an array in the receiver was found to be effective in terms of communication quality. The simulation results confirmed the experimental results, and they support the effectiveness of multichannel OSDM.

Now we will compare OSDM and the other communication schemes. In the single-channel conditions, in terms of communication quality, single-carrier DFE achieved the best quality. OSDM performed almost as well as block- and comb-type OFDM in both Case #1 and Case #2. In light of these results, for the single-channel case, single-carrier DFE and OFDM are attractive in terms of communication quality and receiver complexity, respectively. However, in the multichannel case, the advantage of OSDM may be greater than those of single-carrier DFE and OFDM. As shown in Figures 13c and 14c, OSDM achieves better BER performance compared to single-carrier DFE while the complexity of OSDM is less than 1/10 and 1/2 of single-carrier DFE in Case #1 and Case #2, respectively, as shown in Table II. This means that OSDM may be a viable alternative to single-carrier DFE in terms of both communication quality and complexity. Moreover, the ISNR of OSDM to achieve a BER of 10^{-3} is 7.5 and 5 dB lower than that of OFDM in Case #1 and Case #2, respectively. Note that even considering the ISNR differences listed in Table III, multichannel OSDM remains attractive. This means that OSDM is more attractive than OFDM in terms of communication quality, but multichannel OFDM is more attractive than OSDM in terms of complexity because its complexity is less than 1/1000 of OSDM.

To summarize, considering the factors of communication quality and calculation complexity, multichannel OSDM is well-suited as a UWA communication scheme in multipath channels, and it achieves better communication quality than the other schemes tested.

D. Performance comparison in dynamic channel with various ISNR

We evaluated the performance of OSDM, single-carrier DFE, and OFDM in a dynamic channel, in which the effects of multipath, Doppler spread, and noise are a problem. The communication was tested in a test tank as described above in Section III.C, but a wave generator of periodic motion was also used to make a Doppler spread. Because we confirmed the advantage of multichannel OSDM, we consider only the multichannel case ($K = 3$) here, and we compare the performances of the communication schemes without any solutions (e.g., channel tracker) to compare them in the simplest state.

First, we focus on the property of the Doppler spread obtained in the channel in this experiment. The continuous sinusoidal signal, whose frequency is the same as the carrier, is input to Tx. An example of the signal obtained from Rx #1 is shown in Figure 15a: the wave height at Rx is superposed to the waveform, which can be eliminated by applying a band-pass filter that passes around the carrier frequency (Fig. 15b). By performing short-time Fourier transform and observing the spectrum broadening, we were able to measure the Doppler spread. Figure 16 shows an example of the spectrum, which can be obtained from the signal whose length corresponds to three frames in Case #2, as shown in Figure 15b. In this experiment, we found that the spectrum can be approximated to the bell-shape.

$$S(f) = \frac{C_b}{1 + a\left(\frac{f}{f_\mathrm{d}}\right)}, \quad C_b = \frac{\sqrt{a}}{\pi f_\mathrm{d}}, \quad |f| \le f_\mathrm{d}, \tag{22}$$

where a is positive scalar. The bell-shape function approximated to the obtained spectrum is also shown in the dotted line in

Figure 16. This bell-shape spectrum is used to express the indoor multi-input multi-output (MIMO) channel in which the Doppler spread assumes reflectors moving in the environment [35]. Because the surface wave acts as a moving reflector, the use of the bell-shape function is considered valid. Based on Ref. [35], we set $a = 9$. The effect of the Doppler spread based on the bell-shape function was also considered in the simulation.

To evaluate the effect of the Doppler spread on the communication schemes, we performed the experiment as follows. The wave-making device was activated at various frequencies, resulting in various wave heights and wave lengths (Table IV). In each frequency, the signal frame which contains random information is transmitted continuously for 100 and 32 frames for Cases #1 and #2, respectively, and the communication is performed five times for each ISNR, as was described in Section III.C. To evaluate the relationship between the BER and the Doppler spread, we used the wave height information obtained in Rx. Figure 15c,d shows an example of received signal. In Figure 15c, the wave height at Rx is superposed to the waveform, as is Figure 15a. The relationship between the BER and the Doppler spread can be mapped by comparing f_d from the sinusoid signal and the BER from the communication signal at the same phase of the wave height. To ensure the frequency resolution, we used the received sinusoid signal — which has a length of 7 and 3 frames and whose center corresponds to the focusing frame in the communication signal —to obtain the Doppler spread for Cases #1 and #2, respectively. Because $S(0)/S(f_d) = 10$ in Eq. (20), the Doppler spread was obtained by measuring the width of the spectrum of the received sinusoid signal, which reaches 1/10 from its peak.

Figures 17 and 18 show the experimental and simulation results in Cases #1 and #2, respectively. In Case #1, the ISNRs in the experiment were 30.3, 20.6, and 10.1 dB, and the ISNRs in the simulation are 30.6, 20.6, and 10.6 dB. In case #2, ISNRs in experiment are 28.1, 17.8, and 8.4 dB, and ISNRs in simulation are 30.7, 20.7, and 10.7 dB. By comparing Case #1 (Fig. 17) and Case #2 (Fig. 18), it is clear that the performance of the multichannel for the Doppler spread in Case #1 is better than in Case #2. One of the reasons for this is the frame length difference [30]. As discussed above in Section II.B, the frame length of OSDM corresponds to the required channel coherence time, and the long frame length results in an increase of channel measurement error when the channel is dynamic.

Now we compare OSDM and the other communication schemes we tested. OSDM in Case #1 is very attractive in terms of communication quality. For example, multichannel OSDM achieved error-free communication up to a Doppler shift of 15 Hz when the ISNR is sufficient (Fig. 17a). Even with a low ISNR, multichannel OSDM achieves the best communication quality (Fig. 17c). The advantage of multichannel OSDM for a dynamic channel was also supported by our simulation. Considering the results described in Section III.C, the robustness of OSDM for a low ISNR is expected to be maintained in a dynamic channel. In Case #2, the advantage of multichannel OSDM for the Doppler spread remains superior to those of the other schemes, regardless of the ISNR. DFE achieves error-free communication within several Hz of Doppler spread; however, it does not exceed OSDM. In OFDM, comb-type achieves better BERs compared to block-type, especially in Case #2. This is because the comb type can update the channel information symbol-by-symbol, whereas the block type cannot update the channel for Q symbols, which results in an increase in channel measurement error when the channel is dynamic.

To summarize, multichannel OSDM is well-suited as a UWA communication scheme in which the effects of a Doppler spread are severe. Therefore, we expect that OSDM will enable UWA communication at practical data rates and levels of complexity in shallow water.

IV. Conclusions

We reported the performance comparison of the OSDM scheme and existing schemes in doubly spread channels. We found that the ill-condition problem exists for conventional OSDM, which employs asingle transducer in the receiver. The introduction of a multichannel receiver was found to be effective against the ill-condition problem. We evaluated OSDM communication by comparing it to existing schemes with single-carrier RLS-DFE and OFDM, in a test tank whose reverberation time extended to almost 60 symbols and a Doppler spread up to 15 Hz. In addition, we compared the performance of these schemes with respect to communication quality, data rate, frame length, and calculation complexity. We found that OSDM with a multichannel receiver is attractive in terms of communication quality; it achieved far better BER performance compared to the other schemes in both static and dynamic channels, although its complexity is less than that of RLS-DFE. We expect that OSDM can become a viable alternative offering a highly reliable communication environment for UWA communication with multipath and Doppler spread (such as shallow water) with practical complexity.

Acknowledgments

We thank Dr. Tomohiro Sekiguchi and Mr. Hideo Iijima of the Terrestrial Environment Research Center of the University of Tsukuba for providing the experimental environment. This work was supported by a Grant-in-Aid for Young Scientists (B) (24760672) from the Japan Society for Promotion of Science (JSPS).

REFERENCES

[1] M. Stojanovic, "Recent advances in high-speed underwater acoustic communications," IEEE Journal of Oceanic Engineering **21**, 125–136 (1996).

[2] P. C. Etter, *Underwater Acoustic Modeling and Simulation*, 3rd ed. (Spon Press, Abingdon, Oxfordshire), p. 94, (2003).

[3] R. S. H. Istepanian and M. Stojanovic, *Underwater Acoustic Digital Signal Processing and Communication Systems* (Kluwer Academic Publishers, Dordrecht), pp.3–7, (2002).

[4] H. Ochi, T. Tsuchiya, Y. Amitani, M. Suzuki and S. Negishi, "Study on color video pictures transmission by digital acoustic signal," in *Proceedings of Conference for Pacific Ocean Environments and Probing*, pp.132–137, (1992).

[5] M. Suzuki, T. Sasaki and T. Tsuchiya, "Digital acoustic image transmission system for deep-sea research submersible," in *Proceedings of OCEANS '92*, 567–570 (1992).

[6] M. Stojanovic, J. Catipovic and J. Proakis, "Phase Coherent Digital Communications for Underwater Acoustic Channels," IEEE Journal of Oceanic Engineering, **19**, 100-111 (1994).

[7] M. Stojanovic, J. A. Catipovic, and J. G. Proakis, "Adaptive multichannel combining and equalization for underwater acoustic communications," Journal of Acoustical Society of America **94**, 1621–1631 (1993).

[8] P. S. D. Tarbit, G. Howe, O. Hinton, A. Adams, and B. Sharif, "Development of a real-time adaptive equalizer for a high-rate underwater acoustic data communication link," in *Proceedings of OCEANS '94*, volume 1, I307–I312 (1994).

[9] G. S. Howe, P. Tarbit, O. Hinton, B. Sharif, and A. Adams, "Sub-sea acoustic remote communications utilizing an adaptive receiving beam former for multipath suppression," in *Proceedings of OCEANS '94*, volume 1, I313–I316 (1994).

[10] M. Stojanovic, J. A. Catipovic, and J. Proakis, "Reduced-complexity multichannel processing of underwater acoustic communication signals," Journal of Acoustical Society of America **98**, 961–972 (1995).

[11] M. Stojanovic, J. Proakis and J. Catipovic, "Performance of High-Rate Adaptive Equalization on a Shallow Water Acoustic Channel," Journal of the Acoustical Society of America, **100**, 2213-2219 (1996).

[12] L. Freitag, M. Grund, S. Singh, S. Smith, R. Christenson, L. Marquis, and J. Catipovic, "A bidirectional coherent acoustic communication system for underwater vehicles," in *Proceedings of OCEANS '98*, volume 1, 482–486 (1998).

[13] H. Ochi, Y. Watanabe, and T. Shimura, "Experiments on Acoustic Communication with Quadrature Amplitude Modulation in Multipath Environment," Japanese Journal of Applied Physics, **43**, 3140–3145 (2004).

[14] T. H. Eggen, A. B. Baggeroer, and J. C. Preisig, "Communication over Doppler spread channels. Part I: Channel and receiver presentation," IEEE Journal of Oceanic Engineering, **25**, 62-71 (2000).

[15] T. H. Eggen, A. B. Baggeroer, and J. C. Preisig, "Communication over Doppler spread channels--Part II: Receiver characterization and practical results," IEEE Journal of Oceanic Engineering, **26**, 612-621 (2001).

[16] S. Coatelan and A. Glavieux, "Design and test of a coding OFDM system on the shallow water acoustic channel," in *Proceedings of OCEANS '95*, volume 3, 2065-2070 (1995).

[17] M. Stojanovic, "Low complexity OFDM detector for underwater acoustic channel," in *Proceedings of OCEANS '06*, 2006.

[18] B. Li, S. Zhou, M. Stojanovic, and L. Freitag, "Pilot-tone based ZP-OFDM demodulation for an underwater acoustic channel," Proc. MTS/IEEE OCEANS '06, 2006.

[19] B. Li, S. Zhou, M. Stojanovic, L. Freitag, and P. Willett, "Multicarrier Communication Over Underwater Acoustic Channels With Nonuniform Doppler Shifts," IEEE J. Oceanic Eng. 33 (2008) 198.

[20] S. F. Mason, C. R. Berger, S. Zhou, and P. Willett, "Detection, Synchronization, and Doppler Scale Estimation with Multicarrier Waveforms in Underwater Acoustic Communication," IEEE Journal on Selected Areas in Communication, **26**, 1638-1649 (2008).

[21] N. Suehiro, C. Han, T. Imoto, and N. Kuroyanagi, “An information transmission method using kronecker product,” in *Proceedings of the IASTED International Conference Communication Systems and Networks*, 206–209 (2002).

[22] N. Suehiro, C. Han, and T. Imoto, “Very efficient wireless usage based on pseudo-coherent addition of multipath signals using kronecker product with rows of DFT matrix,” in *Proceeding of the International Symposium on Information Theory*, 385 (2003).

[23] N. Suehiro, R. Jin, C. Han, and T. Hashimoto, “Performance of very efficient wireless frequency usage system using kronecker product with rows of DFT matrix,” in *Proceedings of 2006 IEEE Information Theory Workshop*, 526–529 (2006).

[24] T. Ebihara and N. Suehiro, “The orthogonal signal division multiplexing and its performance evaluation,” IEICE Transactions [in Japanese] **J91-B**, 1086–1094 (2008).

[25] T. Ebihara, K. Mizutani, and N. Wakatsuki, “Basic study of orthogonal signal division multiplexing for underwater acoustic communication: A comparative study,” Japanese Journal of Applied Physics, **49**, 07HG09_01–07HG09_08 (2010).

[26] T. Ebihara and K. Mizutani, “Evaluation of Underwater Acoustic Communication with an Orthogonal Signal Division Multiplexing in Test-tank,” in *Proceedings of the Pacific Rim Underwater Acoustic Conference (PRUAC) 2011*, 57–60, (2011).

[27] M. Sandell, J.V.D. Beek, and P.O. Borjesson, “Timing and frequency synchronization in OFDM systems using the cyclic prefix,” in *Proceedings of International Symposium on Synchronization*, 16-19 (1995).

[28] T. Ebihara and K. Mizutani, “Study of Doppler Shift Correction for Underwater Acoustic Communication Using Orthogonal Signal Division Multiplexing,” Japanese Journal of Applied Physics, **50**, 07HG06_1- 07HG06_8 (2011).

[29] T. Ebihara, “Multichannel Underwater Acoustic Communication with Orthogonal Signal Division Multiplexing on Moving Platform,” in *Proceedings of the 19th International Congress on Sound & Vibration (ICSV19)*, CD-ROM, (2012).

[30] T. Ebihara and K. Mizutani, “Experimental Study of Doppler Effect for Underwater Acoustic Communication Using Orthogonal Signal Division Multiplexing,” Japanese Journal of Applied Physics, **51**, 07GG04_01–07GG04_07 (2012).

[31] S. Zhou, G. B. Giannakis, and C. L. Martret, “Chip-Interleaved Block-Spread Code Division Multiple Access,” IEEE Trans. Communications **50**, 235-248 (2002).

[32] C. Han, N. Suehiro, and T. Hashimoto, “Study of OSDM over Quasi-Static Channel,” The Institute of Electronics, Information and Communication Engineers (IEICE) Technical Report, RCS2007-35, 37-42 (2007).

[33] A. Goldsmith, *Wireless Communications* (Cambridge University Press, Cambridge), p.367, (2005).

[34] H. Sasaoka, *Mobile Communications* (Ohmsha, Tokyo), pp.242–243, (2000).

[35] IEEE P802.11 Wireless LANs, “TGn Channel Models”, IEEE 802.1103/940r4, 2004-05-10.

Figure and Table Captions

FIG. 1. Block diagram of OSDM in the (a) transmitter and (b) receiver.

FIG. 2. Histogram of the condition number when $M = 63$ and $N = 2$.

FIG. 3. Signaling structure for (a) OSDM, (b) single-carrier DFE, and (c) OFDM.

FIG. 4. Block diagram of multichannel RLS-DFE.

FIG. 5. Pilot allocation for OFDM; (a) block-type and (b) comb-type.

FIG. 6. Block diagram of OFDM receiver with maximal ratio combining.

FIG. 7. Testing environment and obtained channel response; (a) testing environment, (b) channel response in the time domain, and (c) channel response in the frequency domain.

FIG. 8. Spectrum of the received signal of (a) OSDM, (b) single-carrier DFE, and (c) OFDM.

FIG. 9. Relationship between training sequence length and OSNR for RLS-DFE; (a) experiment and (b) simulation.

FIG. 10. Relationship between number of array element for receiver K and OSNR; (a) Case #1, experiment, (b) Case #1, simulation, (c) Case #2, experiment, and (d) Case #2, simulation.

FIG. 11. Histograms of PAPR of (a) OSDM and (b) OFDM.

FIG. 12. Output of the transmitter; (a) OSDM and (b) single-carrier in Case #1.

FIG. 13. Relationship between ISNR and BER in Case #1: (a) $K = 1$, experiment, (b) $K = 1$, simulation; (c) $K = 3$, experiment, and (d) $K = 3$, simulation.

FIG. 14. Relationship between ISNR and BER in Case #2: (a) $K = 1$, experiment, (b) $K = 1$, simulation, (c) $K = 3$, experiment, and (d) $K = 3$, simulation.

FIG. 15. Doppler spread measurement in experiment in Case #2: (a) received signal when input: sinusoid signal, (b) bandpass-filtered signal of (a), (c) received signal when input: OSDM signal, and (d) bandpass-filtered signal of (c).

FIG. 16. Example of the spectrum obtained in the experiment (solid line) and approximated bell-shape function (dotted line).

FIG. 17. Relationship between the Doppler spread and the BER in Case #1: ISNR ~ 30 dB (a) $K = 3$, experiment, (b) $K = 3$, simulation, ISNR ~ 20 dB (c) $K = 3$, experiment, (d) $K = 3$, simulation, and ISNR ~ 10 dB (e) $K = 3$, experiment, (f) $K = 3$, simulation.

FIG. 18. Relationship between the Doppler spread and the BER in Case #2: ISNR ~ 30 dB (a) $K = 3$, experiment, (b) $K = 3$, simulation, ISNR ~ 20 dB (c) $K = 3$, experiment, (d) $K = 3$, simulation, and ISNR ~ 10 dB (e) $K = 3$, experiment, (f) $K = 3$, simulation.

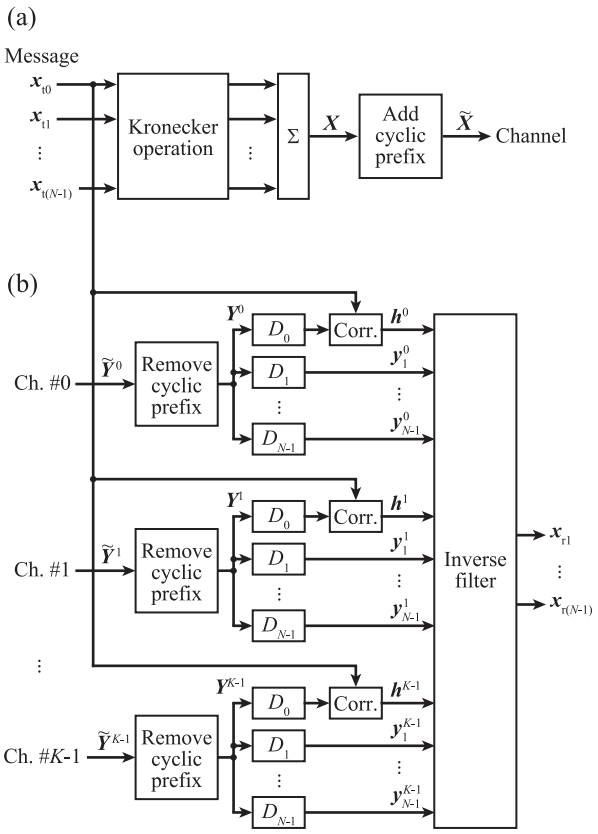
(a)
Message
Kronecker operation
Σ
X
Add cyclic prefix
Channel
(b)
Ch. #0
Ch. #1
Ch. #K-1
Remove cyclic prefix
Corr.
Inverse filter

FIGURE 1

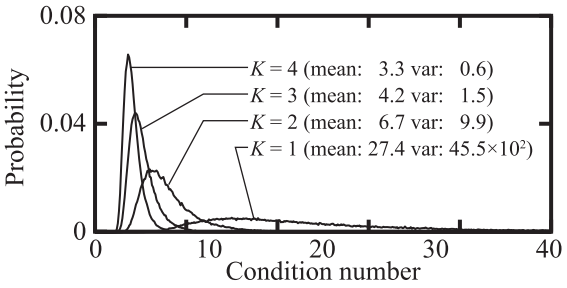
0.08
0.04
0
Probability
0
10
20
30
40
Condition number
K = 4 (mean: 3.3 var: 0.6)
K = 3 (mean: 4.2 var: 1.5)
K = 2 (mean: 6.7 var: 9.9)
K = 1 (mean: 27.4 var: 45.5×10²)

FIGURE 2

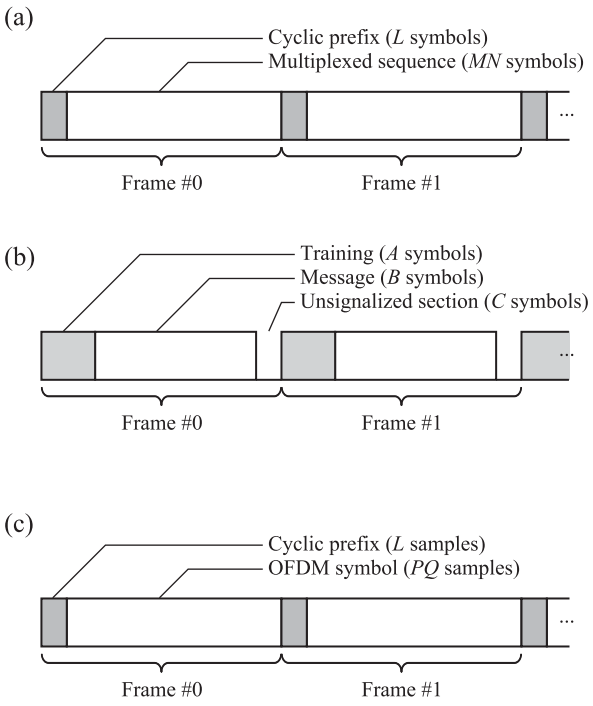
(a)
Cyclic prefix (L symbols)
Multiplexed sequence (MN symbols)
...
Frame #0
Frame #1
(b)
Training (A symbols)
Message (B symbols)
Unsignalized section (C symbols)
...
Frame #0
Frame #1
(c)
Cyclic prefix (L samples)
OFDM symbol (PQ samples)
...
Frame #0
Frame #1

FIGURE 3

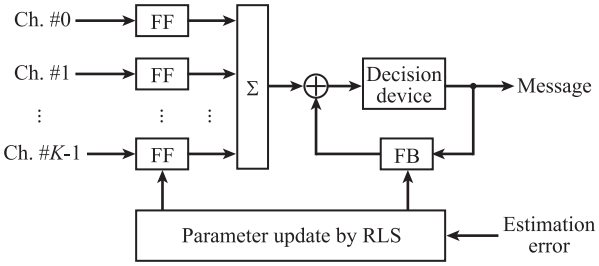
Ch. #0
FF
Ch. #1
FF
Ch. #K-1
FF
Σ
Decision device
Message
FB
Parameter update by RLS
Estimation error

FIGURE 4

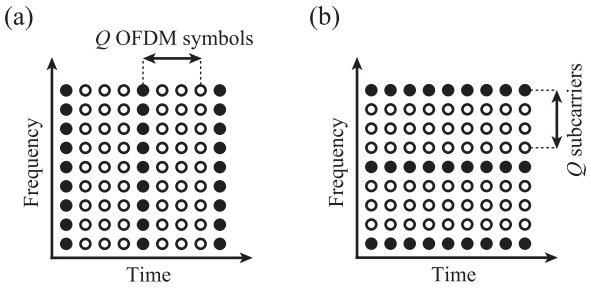
(a)
Q OFDM symbols
Frequency
Time
(b)
Frequency
Q subcarriers
Time

FIGURE 5

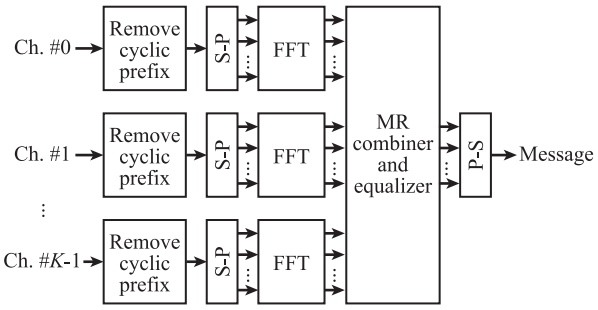
Ch. #0
Remove cyclic prefix
S-P
FFT
Ch. #1
Remove cyclic prefix
S-P
FFT
Ch. #K-1
Remove cyclic prefix
S-P
FFT
MR combiner and equalizer
P-S
Message

FIGURE 6

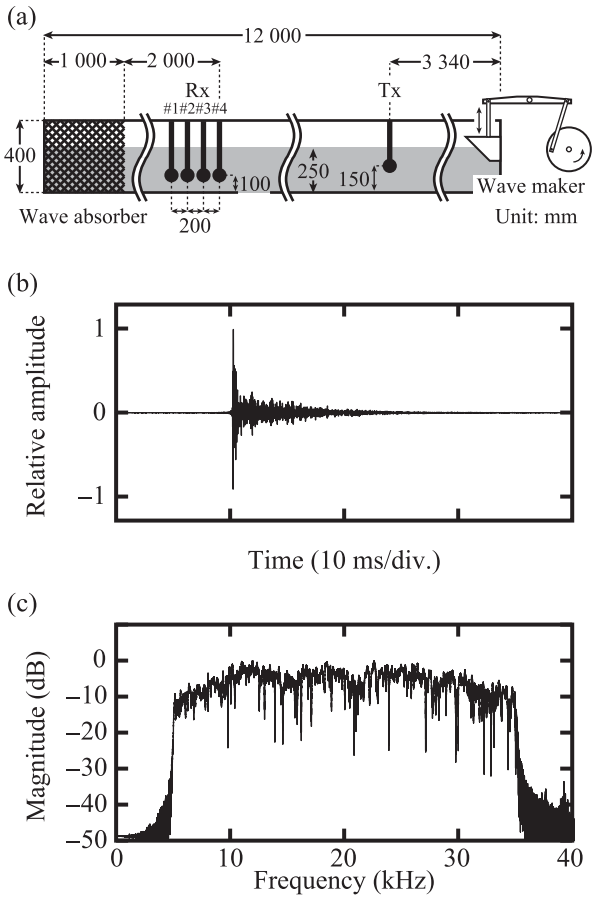
(a)
12 000
1 000
2 000
3 340
Rx
#1#2#3#4
Tx
400
100
250
150
Wave absorber
200
Wave maker
Unit: mm
(b)
Relative amplitude
1
0
−1
Time (10 ms/div.)
(c)
Magnitude (dB)
0
−10
−20
−30
−40
−50
0
10
20
30
40
Frequency (kHz)

FIGURE 7

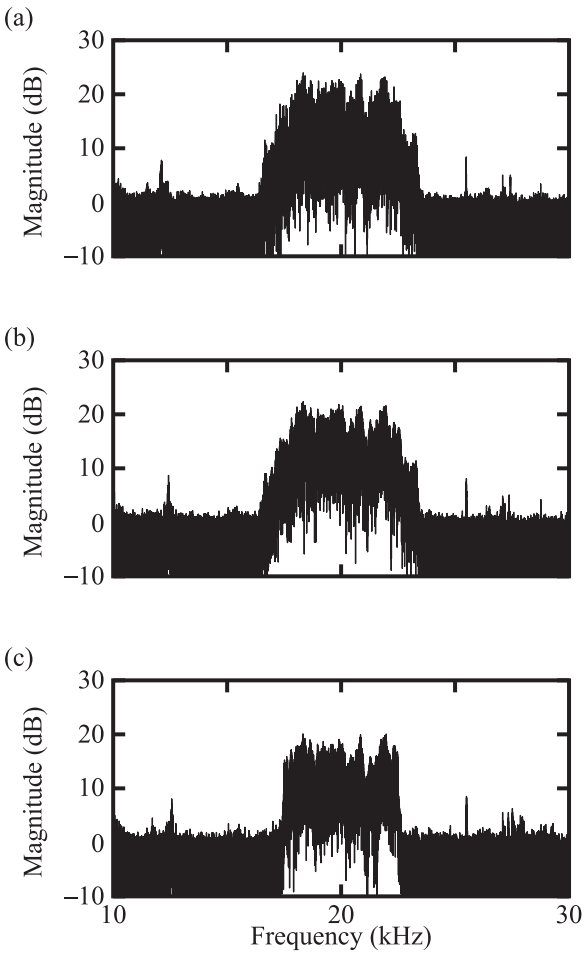
(a)
30
20
10
0
−10
Magnitude (dB)
(b)
30
20
10
0
−10
Magnitude (dB)
(c)
30
20
10
0
−10
Magnitude (dB)
10
20
30
Frequency (kHz)

FIGURE 8

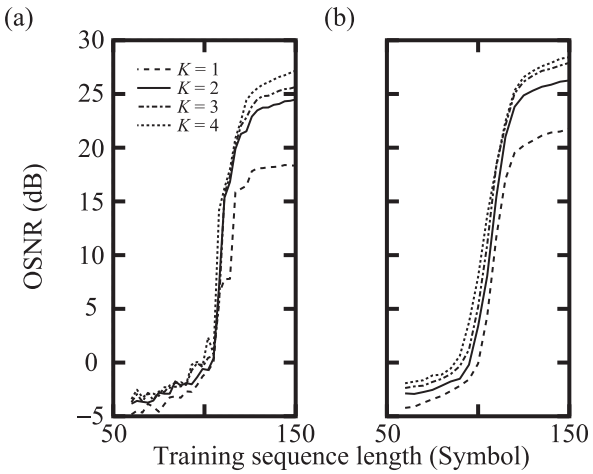
(a)
(b)
30
25
20
15
10
5
0
−5
OSNR (dB)
K = 1
K = 2
K = 3
K = 4
50
150
50
150
Training sequence length (Symbol)

FIGURE 9

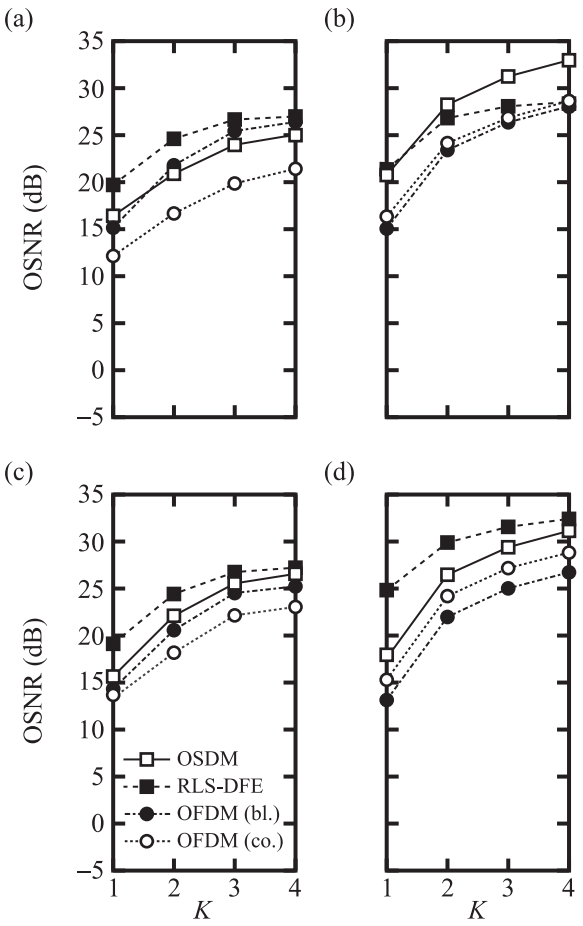
(a)
(b)
(c)
(d)
OSNR (dB)
OSNR (dB)
35
30
25
20
15
10
5
0
–5
1
2
3
4
K
K
OSDM
RLS-DFE
OFDM (bl.)
OFDM (co.)

FIGURE 10

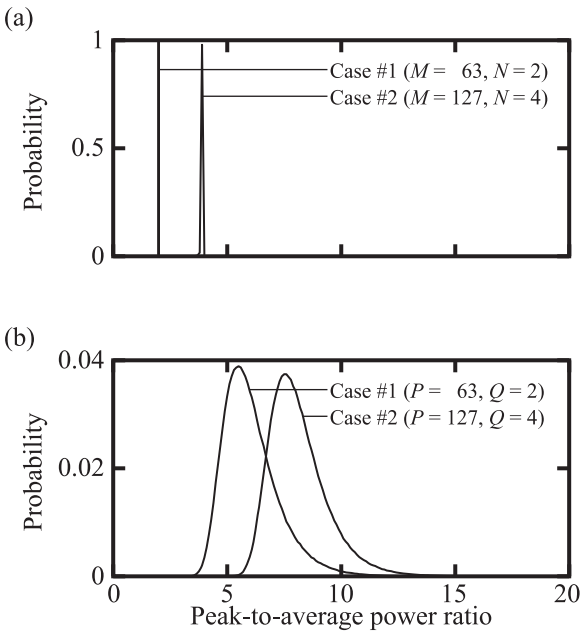
(a)
1
0.5
0
Probability
Case #1 (M = 63, N = 2)
Case #2 (M = 127, N = 4)
(b)
0.04
0.02
0
Probability
Case #1 (P = 63, Q = 2)
Case #2 (P = 127, Q = 4)
0
5
10
15
20
Peak-to-average power ratio

FIGURE 11

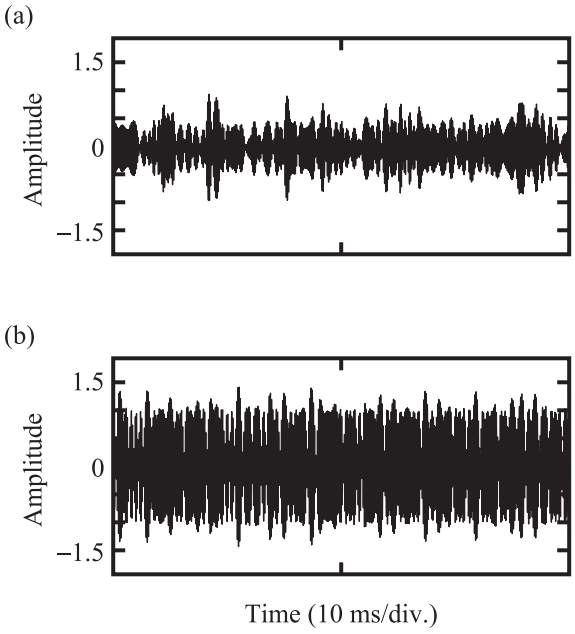

FIGURE 12

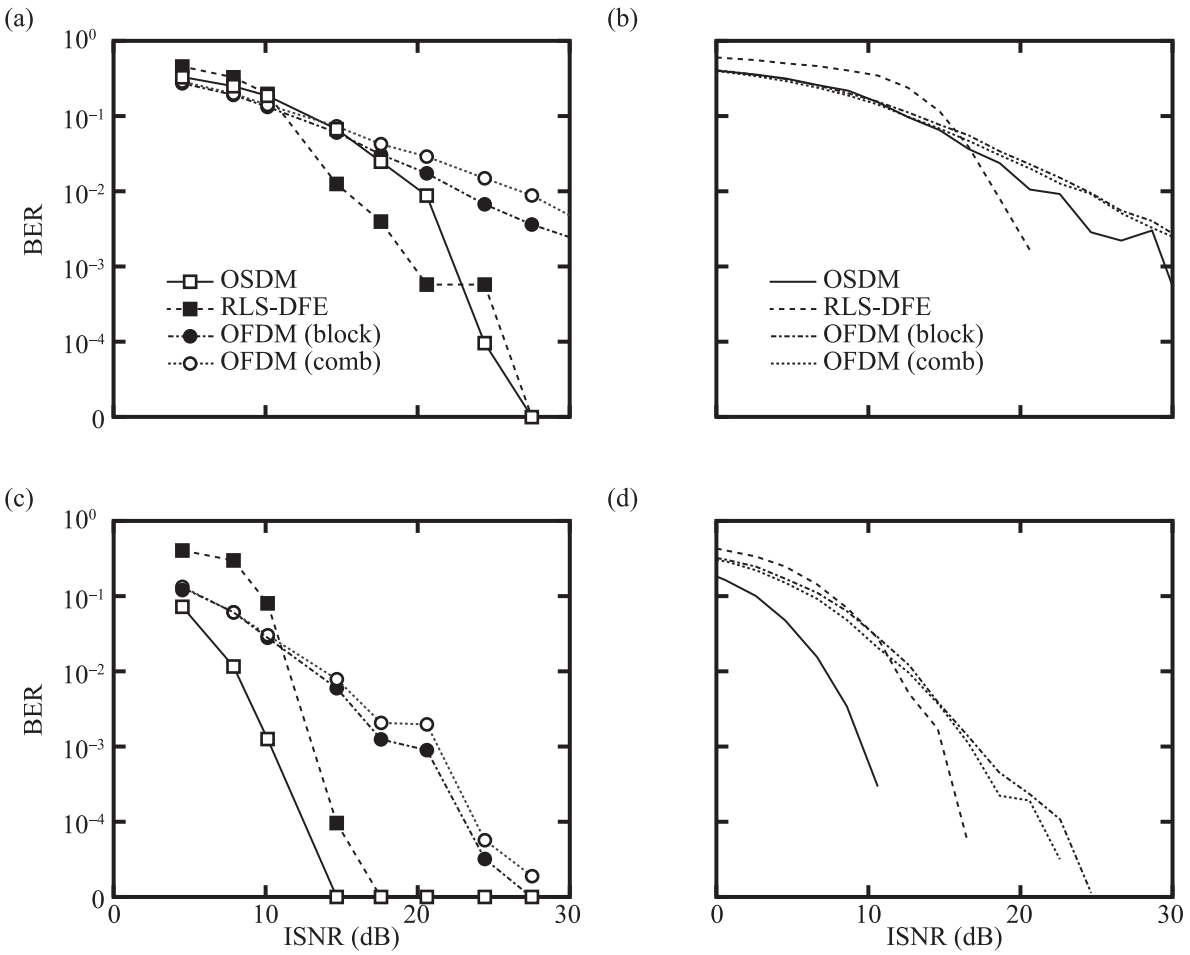
(a)
(b)
(c)
(d)
BER
ISNR (dB)
OSDM
RLS-DFE
OFDM (block)
OFDM (comb)
10^0
10^{-1}
10^{-2}
10^{-3}
10^{-4}
0
10
20
30

FIGURE 13

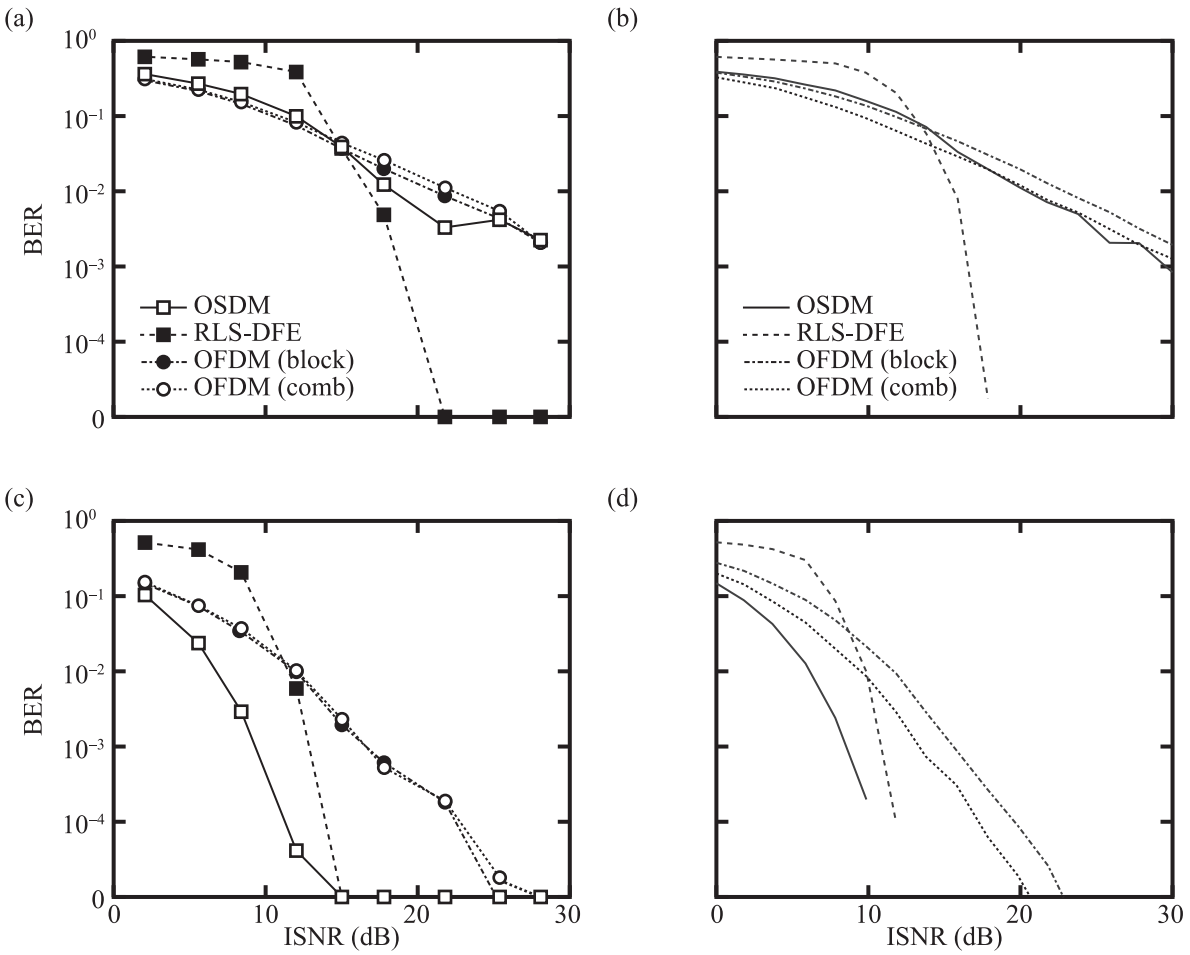
(a)
(b)
(c)
(d)
BER
ISNR (dB)
OSDM
RLS-DFE
OFDM (block)
OFDM (comb)
10^0
10^{-1}
10^{-2}
10^{-3}
10^{-4}
0
10
20
30

FIGURE 14

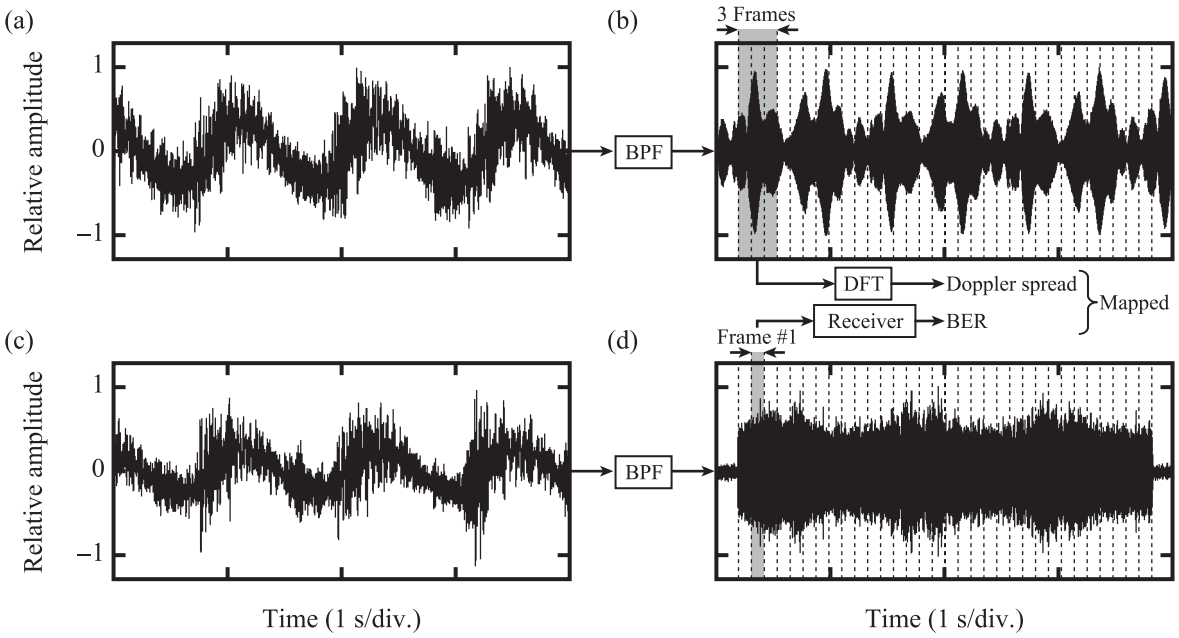
(a)
(b)
3 Frames
Relative amplitude
1
0
−1
BPF
DFT
Doppler spread
Receiver
BER
Mapped
(c)
(d)
Frame #1
Relative amplitude
1
0
−1
BPF
Time (1 s/div.)
Time (1 s/div.)

FIGURE 15

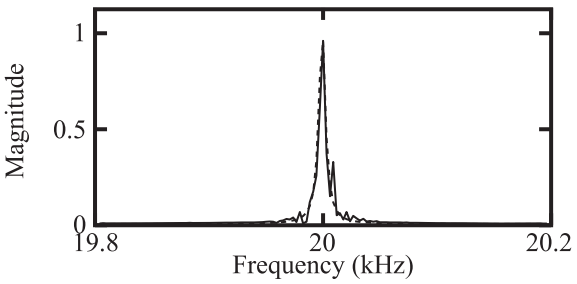

FIGURE 16

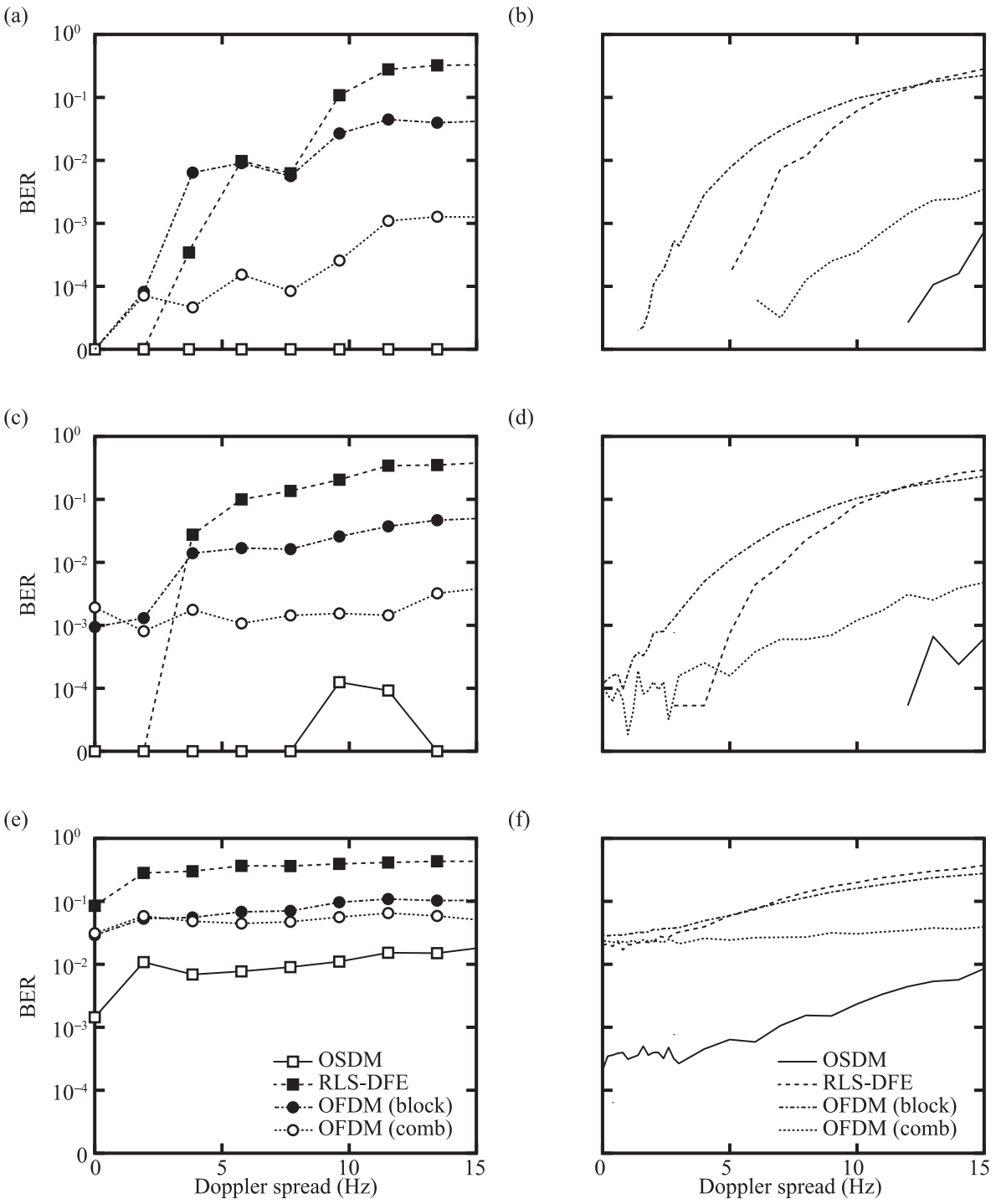
(a)
(b)
(c)
(d)
(e)
(f)
BER
10^0
10^{-1}
10^{-2}
10^{-3}
10^{-4}
0
0
5
10
15
Doppler spread (Hz)
OSDM
RLS-DFE
OFDM (block)
OFDM (comb)

FIGURE 17

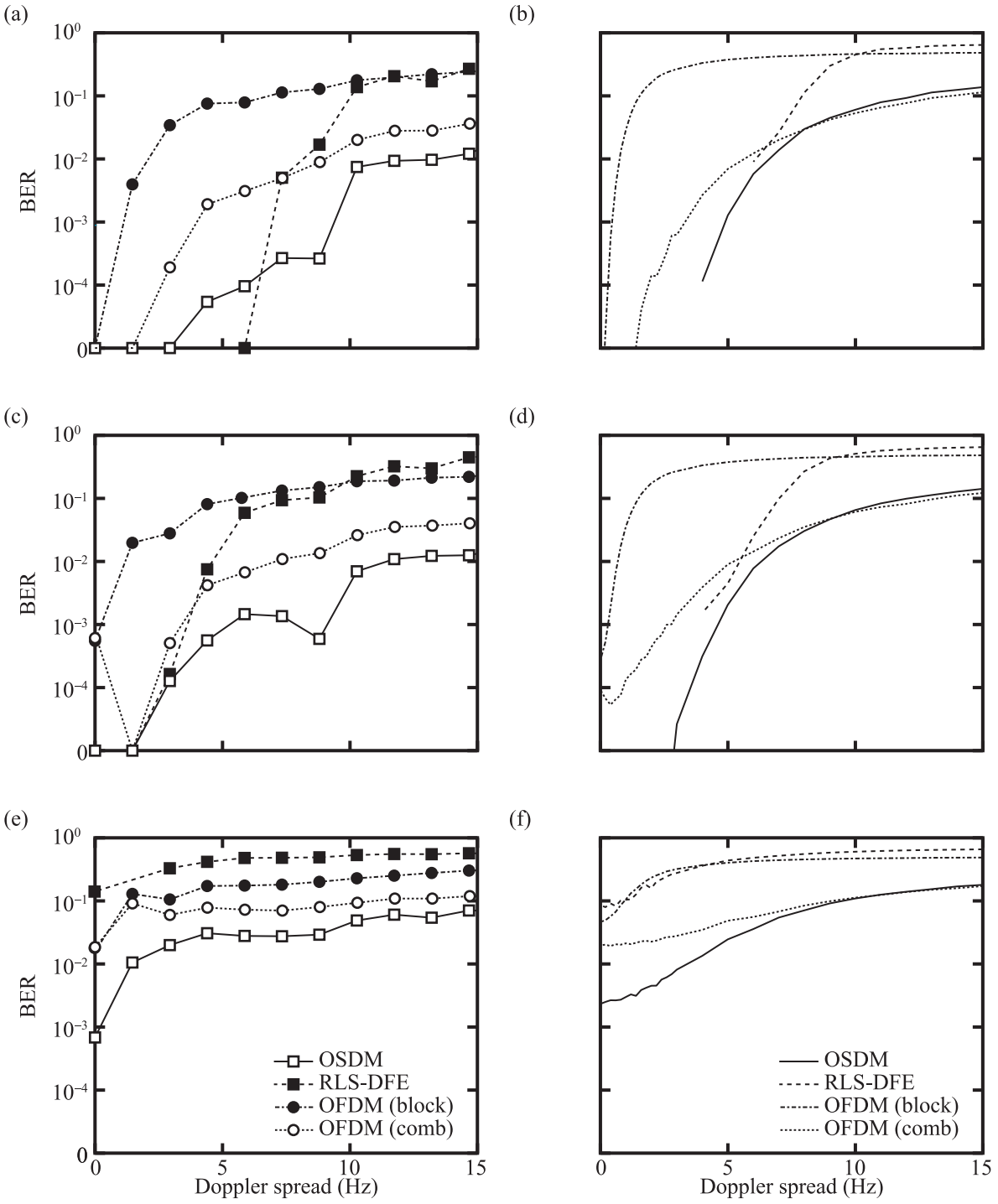
(a)
(b)
(c)
(d)
(e)
(f)
BER
10^0
10^{-1}
10^{-2}
10^{-3}
10^{-4}
0
0
5
10
15
Doppler spread (Hz)
OSDM
RLS-DFE
OFDM (block)
OFDM (comb)

FIGURE 18

TABLE I

Scheme	Data rate	Frame length	Multiplications per frame
OSDM	$\frac{b \cdot M(N-1)}{T(MN+L)}$	$(MN+L)T$	$KN(M^3+M^2)$
Single-carrier RLS-DFE	$\frac{b \cdot B}{T(A+B+C)}$	$(A+B+C)T$	$\left(\frac{5}{2}R^2+\frac{9}{2}R\right)(A+B)$ $R=K(L+1)+L$
OFDM	$\frac{b \cdot P(Q-1)}{T_s(PQ+L)}$	$(PQ+L)T_s$	$\frac{1}{2}KPQ\log_2 PQ$

OSDM, orthogonal signal division multiplexing; RLS-DFE, recursive least-squares-decision feedback equalizer; OFDM, orthogonal frequency division multiplexing

TABLE II

	Type	Parameters	Multiplications (per frame)	Frame length, data rate, and signal bandwidth
Case #1	OSDM	M 63 N 2 L 60	5.0×10^5 (K = 1) 15.3×10^5 (K = 3)	Frame length: 37.2 ms Data rate (QPSK): 3.3 kbps Signal bandwidth: 5 kHz
	Single-carrier DFE	A 123 B 63 C 0	46.8×10^5 (K = 1) 187.3×10^5 (K = 3)	
	OFDM	P 63 Q 2 L 60	4.4×10^2 (K = 1) 1.3×10^3 (K = 3)	
Case #2	OSDM	M 127 N 4 L 60	8.2×10^6 (K = 1) 24.7×10^6 (K = 3)	Frame length: 113.6 ms Data rate (QPSK): 6.7 kbps Signal bandwidth: 5 kHz
	Single-carrier DFE	A 127 B 381 C 60	18.8×10^6 (K = 1) 75.5×10^6 (K = 3)	
	OFDM	P 127 Q 4 L 60	2.3×10^3 (K = 1) 6.8×10^3 (K = 3)	

TABLE III

	Type	ISNR difference from OSDM (Simulation)	ISNR difference from OSDM (Experiment)
Case #1	OSDM	0	0
	Single-carrier DFE	+3.11	+1.63
	OFDM	-4.23	-2.81
Case #2	OSDM	0	0
	Single-carrier DFE	+6.04	+3.75
	OFDM	-2.32	-1.95

TABLE IV

Frequency (Hz)	Wave height (m)	Wave length (m)
1.03	0.08	1.2
0.84	0.06	1.7
0.62	0.05	1.9
0.41	0.02	4.9
0.20	0.02	5.9